Journal of Molecular Graphics and Modelling 42 (2013) 1–6

Contents lists available at SciVerse ScienceDirect

Journal of Molecular Graphics and Modelling

journal homepage: www.elsevier.com/locate/JMGM

Mixed Monte Carlo/Molecular Dynamics simulations of the prion protein

Andre A.S.T. Ribeiro*, Ricardo B. de Alencastro

Instituto de Quimica, Universidade Federal do Rio de Janeiro sala 609, bloco A, Centro de Tecnologia, Cidade Universitaria, Ilha do Fundao, Rio de Janeiro, RJ 21941-909, Brazil

ARTICLE INFO

Article history:
Accepted 15 February 2013
Available online 26 February 2013

Keywords:
Monte Carlo
Molecular Dynamics
Enhanced sampling
GROMACS
Prion misfolding

ABSTRACT

In this paper we present the results of mixed Monte Carlo/Molecular Dynamics (MC/MD) simulations of the D178N mutant of the human prion protein. We have used the MC moves for polypeptide sampling known as Concerted Rotations with Angles (CRA) to selectively sample the region of the prion protein comprising the β-sheet and one of the α-helices. The results indicate that the MC/MD simulations sample the phase space substantially faster than regular Molecular Dynamics simulations starting with the same initial conditions. This work further indicates the MC/MD technique as a potentially powerful simulation tool, allowing the selective sampling of a region of a physical system that is deemed important.

1. Introduction

We have recently reported the results of mixed Monte Carlo/Molecular Dynamics (MC/MD) simulations of a small alanine polypeptide in explicit water [1]. It was shown that the proposed methodology yielded increased sampling when compared to conventional Molecular Dynamics (MD) simulations. The MC/MD method combines the MC moves for peptide sampling known as Concerted Rotations with Angles (CRA) [2–4] with regular MD simulations. The employed MC moves change dihedral and bond angles of four consecutive amino acid residues (i to $i+3$, with i randomly chosen at each MC move). To enforce the local character of the move, two steps are performed. A pre-rotation step changes internal coordinates of most atoms involved in the CRA move, with the exception of the carbonyl group of residue $i+3$. The subsequent chain-closure step determines the coordinates of these two atoms numerically, subjected to some geometric constraints (distances and some bond/dihedral angles should be kept fixed). Due to these constraints, a chain-closure attempt will not necessarily be succesful. Therefore, a Gaussian bias is used during the pre-rotation, with the goal of minimizing the displacement of the last backbone atom involved in this step (C_α of residue $i+3$) [2]. It has been shown that MC simulations employing the CRA moves can lead to efficiency comparable to regular MD in implicit solvent [3].

The MC/MD simulations thus involve the realization of a number of MD steps followed by an MC/CRA step. During the MC step, all atomic velocities are kept fixed. The main advantage of this type of method is the possibility of selectively sampling some degrees of freedom during the MC steps, while allowing the remaining parts of the system to relax during the MD steps.

The results of Ref. [1] were highly encouraging, however, the simplicity of the studied system did not allow a generalization with regards to the usefulness of the methodology. The main problem that could arise in MC/MD simulations of more complex peptides or proteins is a diminished efficiency due to larger side chains or lower solute–solvent distances as a consequence of increased hydrophilicity. In this paper we report results of MC/MD simulations of a significantly more complex system, namely the D178N mutant of the human prion protein.

A conformational transition of the prion protein, from its cellular form (PrP^C) to the misfolded scrapie form (PrP^{Sc}), is thought to be responsible for a class of neurological diseases known as transmissible spongiform encephalopathies [5]. These include Creutzfeldt–Jakob disease and kuru in humans, scrapie in sheep and bovine spongiform encephalopathy and can arise spontaneously or as a result of infection or inheritance of specific mutations. The infectivity of such diseases is known to be caused by the autocatalytic replication of PrP^{Sc} through misfolding of additional PrP^C molecules [6].

The mature human PrP^C is a glycoprotein that consists of a flexible N-terminal region (residues 23–124) and a globular domain in the C-terminal region (residues 125–228) (Fig. 1). This domain is characterized by the presence of three α-helices, H1 (residues 144–153), H2 (residues 173–194) and H3 (residues 200–228), and two short β-strands, S1 (residues 129–130) and S2 (residues 162–163), that form an antiparallel β-sheet [7]. There are a number of interactions that stabilize the PrP^C form, and perturbations in the residues involved in these interactions, such as those caused by pathogenic mutations [8] or decreased pH [9], are associated with

* Corresponding author.
E-mail address: aastr@iq.ufrj.br (A.A.S.T. Ribeiro).

1093-3263/$ – see front matter © 2013 Elsevier Inc. All rights reserved.
http://dx.doi.org/10.1016/j.jmgm.2013.02.007

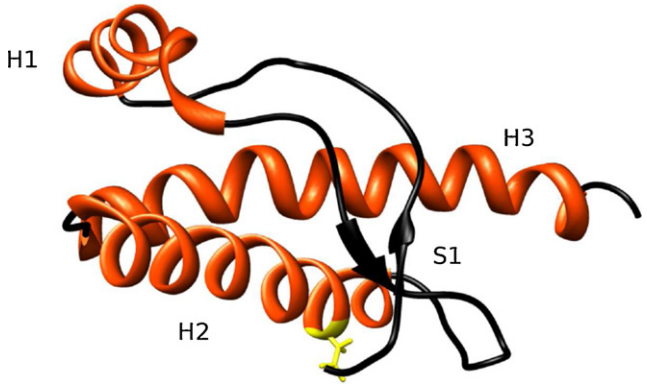

Fig. 1. Starting structure for the MD and MC/MD simulations. Residue Asn 178 is shown in yellow. (For interpretation of the references to color in this figure legend, the reader is referred to the web version of this article.)

PrP^{Sc} formation. The mechanism by which this transition occurs is not completely understood, but it is known to involve a significant increase of β-structure and decrease of helical content [10].

The importance of prion diseases as well as the relatively small size of the prion protein have motivated several theoretical investigations. Metadynamics simulations showed that the D178N mutant, which is involved in a large number of disease cases [11], has a substantially weaker β-sheet than the wild-type protein [12]. This behavior would be in accordance with experimental studies that support a parallel β-fold for PrP^{Sc} [13]. Replica exchange Molecular Dynamics simulations of the globular domain of the wild-type protein at neutral pH showed partially unfolded states characterized by a stable core consisting of helices H2 and H3, while helix H1, although stable, exhibited increased plasticity, moving around the H2–H3 core [14]. More recently, constant-pH MD simulations showed substantial loss of helical content at low pH, with H1 being particularly unstable [15]. This observation is in accordance with experimental findings that indicate a probable refolding of H1 into β-structure upon PrP^{Sc} formation [13,16–18]. Theoretical considerations also indicate the possible importance of this helix to PrP misfolding [19]. Hirschberger and coworkers have also seen unfolding of H1 during MD simulations of the M205S/R mutants [20]. This structural decay occurred after the detachment of H1 from H3 and its subsequent exposure to the aqueous environment. MD simulations of a peptide comprising H1 residues revealed its unfolding kinetics to strongly depend on the dielectric constant of the solvent, with unfolding in water being significantly faster than in less polar solvents [21].

2. Methodology

2.1. System preparation

The NMR structure of wild-type recombinant human protein at neutral pH (PDB code: 1HJM) [22] was used to prepare the initial structure for the simulations. The substitution of Asp178 by Asn was done with the program SWISS PDB-Viewer [23]. The NMR structure utilized, as well as most other NMR structures of recombinant PrPs of different lengths, does not contain coordinates for the atoms of the flexible N-terminal region. There exists experimental evidence indicating the importance of this region to prion misfolding and aggregation [24] and recent MD simulations have included residues 90–124 [25,26,15]. Nevertheless, we are here mainly interested in comparing the sampling capabilities of MC/MD and MD simulations. We have therefore chosen not to include the N-terminal region in our simulations, which would significantly increase the computational cost. The simulated system thus comprises residues 125–228. All simulations were carried out with a modified version of the GROMACS simulation package [1,27]. We have chosen to protonate the sidechains as to reproduce a neutral pH. To this end, we have set all histidine residues as unprotonated, in accordance with the pK_a values calculated by Campos et al. [15].

The prepared structure was solvated with approximatelly eight thousand SPC water molecules in a truncated dodecahedral box. The simulation setup included energy minimization steps with the *steepest descents* algorithm followed by a 500 ps position restrained MD simulation to accomodate water molecules around the solute. The GROMOS96 53a6 force-field [28] was utilized with long-range electrostatic interactions being treated with the particle-mesh Ewald (PME) method.

2.2. MC/MD and MD simulations

A total of twenty 100 ns simulations were performed. Some of these simulations were extended as discussed below. All simulations started from the same initial coordinates, although with different initial velocities. The simulations were divided in ten pairs, each one consisting of one MC/MD and one MD simulation starting with the same initial velocities. Simulations were carried out in the NVT ensemble at 300 K with the velocity-rescaling algorithm of Bussi et al., with a time constant of 0.1 ps [29]. Bond lengths were constrained with the LINCS algorithm [30]. The leap frog algorithm was used to integrate the equations of motion, with an integration step of 2 fs.

It must be noted that the MC/MD and MD simulations performed the same number of simulation steps (50×10^6). The time of an MC/MD simulation is obviously not well defined. We have chosen to express the total number of simulation steps as "simulation time" for convenience. All simulations were run in parallel.

The main advantage (and problem) of Monte Carlo simulations/moves is the freedom they provide for sampling the configurational space. We believe that MC/MD can be a powerful simulation technique, allowing the possibility of increased sampling of a particular region of the system that is deemed important. We have therefore chosen to perform MC/CRA moves of several residues in the S1–H1–S2 region. MC/MD simulations performed one MC/CRA step after each 100 simulation steps. The parameters that determine the amplitude of the CRA moves were the same as in Ref. [1] and the resulting acceptance ratios will be discussed below. As in Ref. [1], we have not observed any temperature discrepancies or violations of the constrained distances. To further illustrate that the use of MC moves in the MC/MD simulations does not generate a significant impact on the velocity distribution, we have conducted two additional 3 ns simulations, one MD and one MC/MD, in which velocities were recorded every 10 simulation steps. The calculated average translational kinetic energies for the atoms belonging to residues involved in the CRA moves (see below) were 3.68 ± 3.01 kJ/mol and 3.71 ± 3.02 kJ/mol for the MD and MC/MD simulations, respectively. The corresponding distributions are shown in Fig. S1, Supporting Information.

A performance measure (8 processes running on an Intel Xeon 2.43 GHz) yielded 9.48 ns/day and 9.39 ns/day for MD and MC/MD, respectively. It must be noted that the slight performance difference is due to increased communication necessary for the MC moves, as a CRA step is computationally cheaper than a MD step on a single processor (data not shown). The employed code has not been optimized to reduce this issue.

Table 1
Average acceptance ratios of the CRA moves in the MC/MD simulations.

Involved residues	Region	Acceptance ratio
Met129-Leu130-Gly131-Ser132	S1	0.324
Gly142-Ser143-Asp144-Tyr145	H1	0.201
Ser143-Asp144-Tyr145-Glu146	H1	0.236
Asp144-Tyr145-Glu146-Asp147	H1	0.242
Tyr145-Glu146-Asp147-Arg148	H1	0.234
Glu146-Asp147-Arg148-Tyr149	H1	0.208
Asp147-Arg148-Tyr149-Tyr150	H1	0.224
Glu160-Val161-Tyr162-Tyr163	S2	0.244

3. Results and discussion

3.1. MC acceptance ratios

As pointed out above, the main concern in using the MC/MD technique on protein simulations amounts to a possible decrease in the efficiency of the MC moves. The employed CRA moves change the ϕ and ψ dihedral angles, as well as some bond angles, of four consecutive amino acid residues [2]. The size of the CRA moves is controlled by three parameters (c_1, c_2, and c_3). The magnitude of the internal coordinate changes during the pre-rotation step is controlled by c_1, while the strength of the applied bias is controlled by c_2. The third parameter controls differences between changes in dihedral and bond angles. As with any other MC move, one needs to adjust these parameters in order to obtain maximal sampling efficiency. In our previous study [1] we have set these parameters to values that yielded an acceptance ratio of 0.36 for dodecaalanine described by the OPLS-AA forcefield [31] and solvated with explicit water molecules. In the present study we have used the same set of parameters ($c_1 = 75$, $c_2 = 8$, $c_3 = 20$), in order to evaluate the effect of longer sidechains on the efficiency of the CRA moves. Table 1 shows the obtained acceptance ratios for each of the eight CRA moves used in this study, averaged over ten 100 ns MC/MD simulations. It must be noted that every MC/MD simulation performed each of the listed MC moves with equal probability.

The results show a slight decrease of the acceptance ratio of the move involving the residues in S1 when compared to the previous polyalanine value. This particular move involves a hydrophilic residue (Ser) and a residue with a significantly longer sidechain than alanine (Met). The other CRA moves involve residues with even longer sidechains and also charged residues (Asp, Glu, Arg). For these moves a significant decrease of acceptance ratios is observed. Nevertheless, the obtained values are not exceedingly low as to render the method necessarily inefficient.

3.2. Secondary structure evolution

We have used the DSSP algorithm [32] to monitor changes in secondary structure during the simulations. The most significant structural change was a decrease in helical content, which was observed in both MC/MD and MD simulations, although to different extents. Fig. 2A shows the total helicity as a function of time, averaged over all simulations of each type. It can be seen that the MC/MD simulations resulted in a more pronounced reduction of helical content. This difference was traced back mainly to the region comprising helix H1 (residues 144–153). Fig. 2B shows the helicity calculated over these residues and averaged over all simulations of each type. The results indicate a significant difference between MC/MD and MD simulations, with MC/MD losing much more helical content in this region, which was subjected to most CRA moves.

The analysis of individual trajectories showed that, while H1 was stable in the MD simulations, its behavior was completely different in three of the MC/MD simulations. These runs displayed a total collapse of H1 after 20–50 ns, with one of these forming a β-bridge between Ile138 and Tyr149 after 85 ns (see below). Visual inspection of the corresponding trajectories shows that the hydrogen bond between Tyr149 and Asp202 is lost prior to H1 unfolding. The emerging picture is an increased solvent exposure of H1 residues after the loss of this hydrogen bond with subsequent H1 unfolding (Fig. 3). This is in accordance with the results of MD simulations of M205S/R mutants [20]. The fact that MC/MD was able to generate this conformational change is probably due to the increased movement of Tyr149, which was subjected to several CRA moves (Table 1).

Several features were present in both MC/MD and MD simulations. These include the partial loss of helix H2 and, to a lesser extent, of H3. These changes were mainly restricted to the C-terminal regions of these helices. A comparison of MC/MD and MD simulations as to structural changes in the H2–H3 core shows that both techniques yield equivalent results (Fig. 4A). Nevertheless, individual simulations still show significant differences (Fig. 4B). In fact, for the two MC/MD simulations that displayed the highest decrease of helical content in the H2–H3 core, one also lost H1 (red curve in Fig. 4B), while the other did not (green curve in Fig. 4B), indicating that loss of helical content in both subdomains is most likely independent. This particular simulation exhibited a substantial loss of helix H2, from its C-terminal region up to Val180 (Fig. S2, Supporting Information).

Both MD and MC/MD simulations displayed a stable β-sheet at S1 and S2, in accordance with the constant-pH MD simulations of Campos and coworkers [15] and in contrast to experimental and theoretical studies of the D178N [12,33] and T183A [34] mutants. The theoretical results indicate that the behavior of this structural element may depend on the simulation protocol employed.

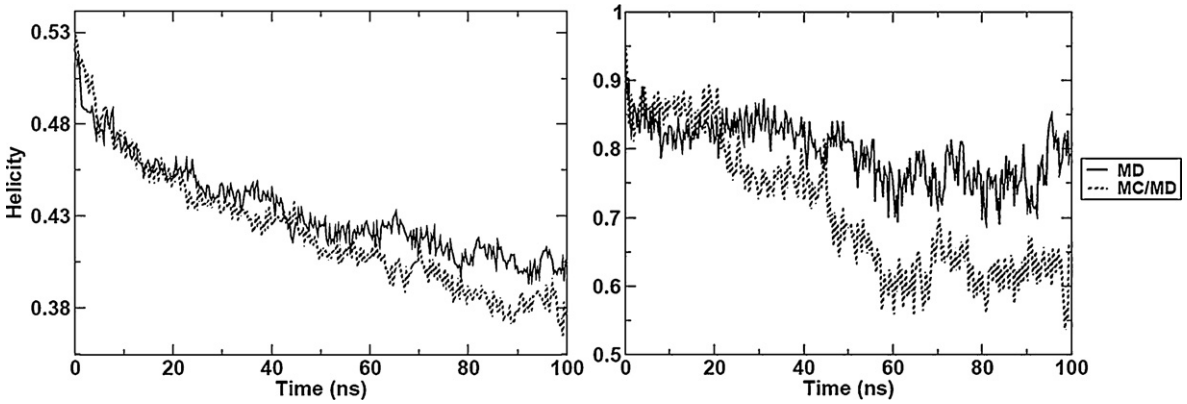

Fig. 2. Helicity as a function of time. (A) Total helicity and (B) helicity over residues comprising helix H1. The displayed results are averaged over all simulations of each type.

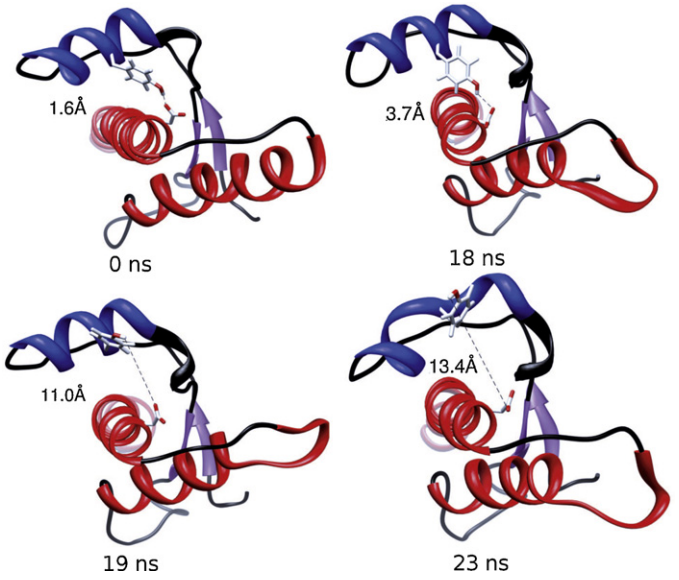

Fig. 3. Snapshots from one of the MC/MD simulations that exhibited H1 collapse. Helix H1 is colored with blue, while helices H2 and H3 are colored with red. The sidechains of Tyr149 and Asp202 are displayed, along with the distance between the atoms that were hydrogen bonded in the initial structure. DSSP analysis indicates that this particular MC/MD simulation exhibited H1 collapse after 22 ns.

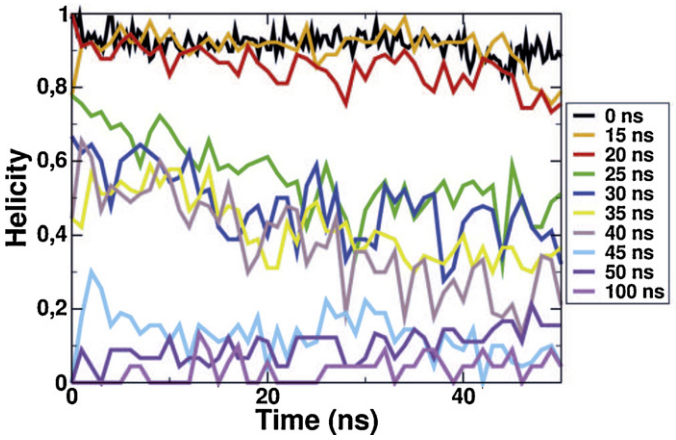

Fig. 5. Secondary structure evolution for the 50 ns MD simulations that started from configurations taken from one of the MC/MD trajectories. Each line represents an average over 10 MD simulations.

3.3. Increased sampling of MC/MD simulations

The difference between the MC/MD and MD simulations clearly stems from the use of the CRA moves to enhance sampling of the H1 region, which was shown above to suffer the most significant structural changes in the simulations. However, for a simulation technique to be useful, it must provide physically meaningful results. Therefore, the observed differences must be due to the MC/MD simulations being able to cross a free energy barrier and the MD simulations remaining trapped in a free energy minimum due to this same barrier. If this is not true, one can conclude that MC/MD is not sampling from the correct statistical distribution. Previous results of simulations of the prion protein in destabilizing conditions, with the same forcefield used in this study [15], indicate that the first scenario is more likely. Nevertheless, we have conducted additional MD simulations to further demonstrate the existence of a free energy barrier corresponding to the collapse of H1, which the MD simulations were not able to cross. To this end, we have performed several 50 ns MD simulations starting from configurations taken from one of the MC/MD trajectories that showed a collapsed helix H1 (which ocurred after approximately 42 ns). Fig. 5 shows the helicity on residues 144–153 as a function of time, averaged over 10 MD simulations. The results show a consistent helicity decrease for the MD simulations taken from times up to 40 ns. The remaining simulations already start from a collapsed H1 and do not refold, even though some do present α-helix formation on residues 144–148. The secondary structure classification of residues 125–169 as a function of time for the MD simulations that started from 40, 45, 50 and 100 ns is shown in the Supporting Information (Figs. S3–S6, respectively).

The results show that MD simulations that start from a collapsed H1 do not exhibit refolding in 50 ns, while MD simulations that start from a folded H1 do not exhibit unfolding in 100 ns. Although this finding provides further evidence of the existence of a free energy barrier for H1 unfolding, it does not prove that the unfolding process amounts to a decrease in free energy at 300 K. To further characterize the free energy surface for H1 unfolding, we have used a well-established increased sampling technique. Well-tempered metadynamics simulations [35] were performed by coupling GROMACS to the PLUMED plugin [36]. The details of the performed simulations are described in the Supporting Text section of the Supporting Information. The free energy as a function of a collective variable S that monitors the

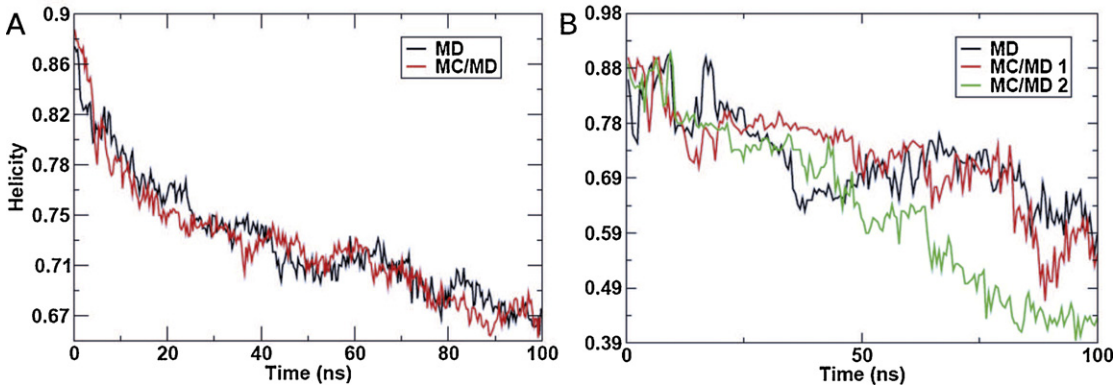

Fig. 4. Helicity over residues comprising the H2–H3 core as a function of time. (A) Averaged over all simulations of each type and (B) results for the MD simulation and the two MC/MD simulations that exhibited the most significant decrease of helical content in this region. (For interpretation of the references to color in the text, the reader is referred to the web version of this article.)

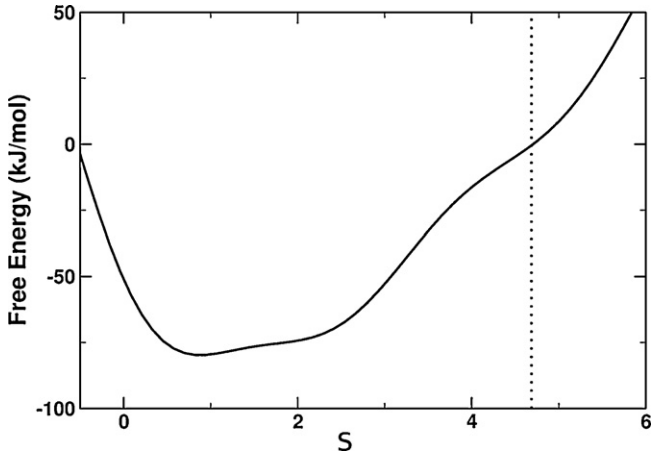

Fig. 6. Free energy surface for H1 unfolding. The collective variable *S* monitors the number of backbone hydrogen bonds between residues comprising helix H1 (see Supporting Text in Supporting Information). The dashed line gives the value of *S* for the starting (folded) structure.

number of hydrogen bonds between H1 residues is shown in Fig. 6. The value of *S* is given as

$$S = \frac{\sum_{ij} 1 - (d_{ij}/r_0)^6}{\sum_{ij} 1 - (d_{ij}/r_0)^{12}},$$

where *i* and *j* denote groups of hydrogen bond donors and acceptors and r_0 was set as its default value of 2.5 (see Supporting Information for further details).

The results indicate that the unfolded state is thermodynamically preferred at 300 K, with an unfolding free energy difference of -13.5 kcal/mol. This result gives solid evidence that the MD simulations at 300 K do not exhibit H1 unfolding in 100 ns due to the existence of a free energy barrier and that the MC/MD simulations are indeed correct. It must be noted that the chosen collective variable does not allow us to calculate this energy barrier (Fig. 6). A more careful analysis, employing other collective variables, would probably be necessary to fully characterize this process.

3.4. Extended MC/MD simulations

The previous results indicate a significant increase in sampling efficiency of the MC/MD technique over regular MD. We have therefore extended to 400 ns two of the MC/MD simulations that displayed H1 collapse, which could possibly reveal further structural changes. We will hereafter refer to these as simulations MC/MD-H1a, MC/MD-H1b. The evolution of the secondary structure for these simulations is shown in Fig. 7, panels A and B, respectively. It can be seen that unfolding of H1 occurred early in both simulations. After this unfolding event, the behavior of the former H1 residues differ substantially. In MC/MD-H1a, residues 144–148 transiently form a π-helix, while in MC/MD-H1b shows the formation of a β-bridge between residues Ile138 and Tyr149 (for a comparison with MD simulations, see Figs. S3–S6 in the Supporting Information). Fig. 7B also shows that residues 144–148 lose any tendency to form helical structures after 290 ns and a β-bridge between residues Phe141 and Tyr150 is formed after 380 ns. These observations indicate that a further structural change occurred in this run. This may be an initial step towards formation of stable β-structure in the region of former helix H1 and is in accordance with the results of Campos et al. [15], who observed significant formation of β-structure in region 135–155 at low pH. The extended simulations also continue to display a stable β-sheet between S1 and S2 and show substantial decrease of helical content in the H2–H3

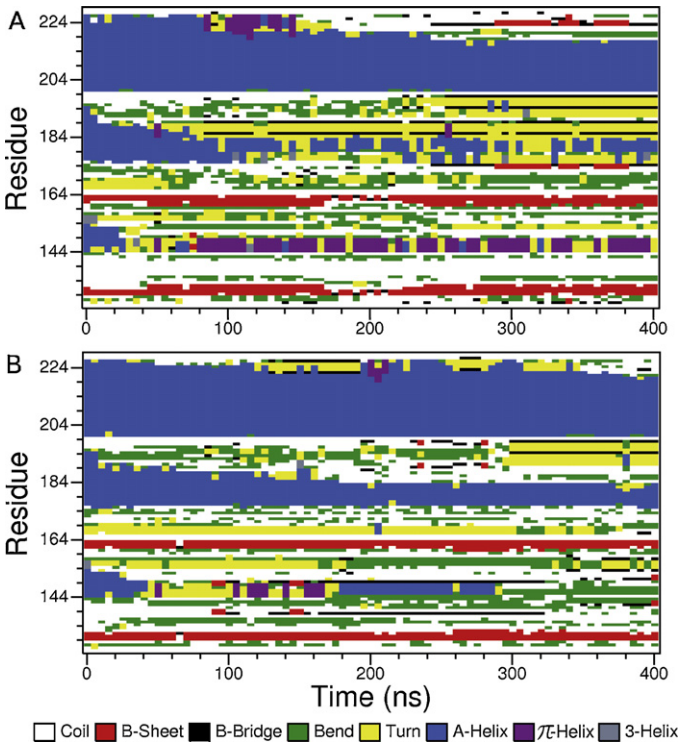

Fig. 7. Secondary structure as a function of time for the simulations (A) MC/MD-H1a and (B) MC/MD-H1b.

core, especially in the C-terminal region of helix H2. This behavior is again in accordance with the results of Campos and coworkers [15], who observed formation of β-structure in residues 185–200. MC/MD-H1a also shows a β-sheet between Asn173-Asn174 and Gln223-Ala224 being transiently formed. The final structure of both simulations is shown in Fig. S7, Supporting Information.

4. Conclusions

In this paper we report the results of MD and MC/MD simulations of the D178N mutant of the human prion protein. It is shown that some MC/MD simulations were able to cross a free energy barrier that resulted in the unfolding of helix H1. This structural change happened after the loss of a specific hydrogen bond between H1 and H3, involving residues Tyr149 and Asp202. This behavior was not observed in any of the MD simulations. The difference most probably stems from the use of the CRA moves in the MC/MD simulations, which selectively sampled residues in the S1–H1–S2 subdomain, including Tyr149. MD simulations starting from a configuration with an unfolded H1 did not display its refolding, further confirming that, while MC/MD was able to cross a free energy barrier, MD was not. Well-tempered metadynamics revealed that the unfolded H1 is thermodinamically more stable at 300 K, providing further evidence on the correctness of the MC/MD simulatins. Extended MC/MD simulations revealed further structural changes that could be an initial step towards formation of β-structure seen elsewhere [15].

Compared to our earlier study on polyalanine systems [1], the results presented here strongly advocate the efficiency of mixed Monte Carlo/Molecular Dynamics simulations. It is shown that this technique can be used to selectively sample regions of a physical system that are deemed important. Furthermore, this is accomplished without the need to modify the Hamiltonian of the system or introduce external forces.

Acknowledgements

The authors would like to thank Prof. Marco A. Chaer do Nascimento for kindly allowing part of the simulations reported here to be run in his laboratory. Financial support from CNPq, CAPES and FAPERJ is acknowledged.

Appendix A. Supplementary Data

Supplementary data associated with this article can be found, in the online version, at http://dx.doi.org/10.1016/j.jmgm.2013.02.007.

References

[1] A.A.S.T. Ribeiro, R.B. de Alencastro, Mixed monte carlo/molecular dynamics simulations in explicit solvent, J. Comput. Chem. 33 (2012) 901–905.
[2] J.P. Ulmschneider, W.L. Jorgensen, Monte carlo backbone sampling for polypeptides with variable bond angles and dihedral angles using concerted rotations and a gaussian bias, J. Chem. Phys. 118 (9) (2003) 4261–4271.
[3] J. Ulmschneider, M. Ulmschneider, A. Di Nola, Monte carlo vs molecular dynamics for all-atom polypeptide folding simulations, J. Phys. Chem. B 110 (33) (2006) 16733–16742.
[4] J. Ulmschneider, M. Ulmschneider, Sampling efficiency in explicit and implicit membrane environments studied by peptide folding simulations, Proteins: Struct. Funct. Bioinf. 75 (3) (2009) 586–597.
[5] S.B. Prusiner, Prions, Proc. Natl. Acad. Sci. U.S.A. 95 (23) (1998) 13363–13383.
[6] F. Cohen, K. Pan, Z. Huang, M. Baldwin, R. Fletterick, S. Prusiner, Structural clues to prion replication, Science 264 (5158) (1994) 530–531.
[7] R. Riek, S. Hornemann, G. Wider, M. Billeter, R. Glockshuber, K. Wüthrich, NMR structure of the mouse prion protein domain prp (121-231), Nature 382 (6587) (1996) 180–182.
[8] M. Van Der Kamp, V. Daggett, The consequences of pathogenic mutations to the human prion protein, Prot. Eng. Des. Sel. 22 (8) (2009) 461–468.
[9] M. DeMarco, V. Daggett, Local environmental effects on the structure of the prion protein, Comp. Rend. Biol. 328 (10–11) (2005) 847–862.
[10] K.M. Pan, M. Baldwin, J. Nguyen, M. Gasset, A. Serban, D. Groth, I. Mehlhorn, Z. Huang, R.J. Fletterick, F.E. Cohen, Conversion of alpha-helices into beta-sheets features in the formation of the scrapie prion proteins, Proc. Natl. Acad. Sci. U.S.A. 90 (23) (1993) 10962–10966.
[11] S. Mead, Prion disease genetics, Eur. J. Hum. Gen. 14 (3) (2006) 273–281.
[12] A. Barducci, R. Chelli, P. Procacci, V. Schettino, F. Gervasio, M. Parrinello, Metadynamics simulation of prion protein: β-structure stability and the early stages of misfolding, J. Am. Chem. Soc. 128 (8) (2006) 2705–2710.
[13] C. Govaerts, H. Wille, S.B. Prusiner, F.E. Cohen, Evidence for assembly of prions with left-handed β-helices into trimers, Proc. Natl. Acad. Sci. U.S.A. 101 (22) (2004) 8342–8347.
[14] A. De Simone, A. Zagari, P. Derreumaux, Structural and hydration properties of the partially unfolded states of the prion protein, Biophys. J. 93 (4) (2007) 1284–1292.
[15] S.R.R. Campos, M. Machuqueiro, A.M. Baptista, Constant-pH molecular dynamics simulations reveal a β-rich form of the human prion protein, J. Phys. Chem. B 114 (39) (2010) 12692–12700.
[16] T. Pan, B. Chang, P. Wong, C. Li, R. Li, S. Kang, J. Robinson, A. Thompsett, P. Tein, S. Yin, G. Barnard, I. McConnel, D. Brown, T. Wisniewiski, M. Sy, An aggregation-specific enzyme-linked immunosorbent assay: detection of conformational differences between recombinant prp protein dimers and prpsc aggregates, J. Virol. 79 (19) (2005) 12355–12364.
[17] E.M. Norstrom, J.A. Mastrianni, The charge structure of helix 1 in the prion protein regulates conversion to pathogenic prpsc, J. Virol. 80 (17) (2006) 8521–8529.
[18] F. Eghiaian, T. Daubenfeld, Y. Quenet, M. van Audenhaege, A.-P. Bouin, G. van der Rest, J. Grosclaude, H. Rezaei, Diversity in prion protein oligomerization pathways results from domain expansion as revealed by hydrogen/deuterium exchange and disulfide linkage, Proc. Natl. Acad. Sci. U.S.A. 104 (18) (2007) 7414–7419.
[19] M. Morrissey, E. Shakhnovich, Evidence for the role of prpc helix 1 in the hydrophilic seeding of prion aggregates, Proc. Natl. Acad. Sci. U.S.A. 96 (20) (1999) 11293–11298.
[20] T. Hirschberger, M. Stork, B. Schropp, K. Winklhofer, J. Tatzelt, P. Tavan, Structural instability of the prion protein upon m205s/r mutations revealed by molecular dynamics simulations, Biophys. J. 90 (11) (2006) 3908–3918.
[21] M. Lingenheil, R. Denschlag, P. Tavan, Highly polar environments catalyze the unfolding of prp c helix 1, Eur. Biophys. J. 39 (8) (2010) 1177–1192.
[22] L. Calzolai, R. Zahn, Influence of pH on NMR structure and stability of the human prion protein globular domain, J. Biol. Chem. 278 (37) (2003) 35592–35596.
[23] N. Guex, M. Peitsch, Swiss-model and the swiss-pdb viewer: an environment for comparative protein modeling, Electrophoresis 18 (15) (1997) 2714–2723.
[24] D. Peretz, R. Williamson, Y. Matsunaga, H. Serban, C. Pinilla, R. Bastidas, R. Rozenshteyn, T. James, R. Houghten, F. Cohen, S. Prusiner, D. Burton, A conformational transition at the n terminus of the prion protein features in formation of the scrapie isoform1, J. Mol. Biol. 273 (3) (1997) 614–622.
[25] M. DeMarco, V. Daggett, Characterization of cell-surface prion protein relative to its recombinant analogue: insights from molecular dynamics simulations of diglycosylated, membrane-bound human prion protein, J. Neurochem. 109 (1) (2009) 60–73.
[26] M. Van der Kamp, V. Daggett, Influence of pH on the human prion protein: insights into the early steps of misfolding, Biophys. J. 99 (7) (2010) 2289–2298.
[27] B. Hess, C. Kutzner, D. Van Der Spoel, E. Lindahl, Gromacs 4: algorithms for highly efficient, load-balanced, and scalable molecular simulation, J. Chem. Theory Comput. 4 (3) (2008) 435–447.
[28] C. Oostenbrink, A. Villa, A. Mark, W. Van Gunsteren, A biomolecular force field based on the free enthalpy of hydration and solvation: the gromos force-field parameter sets 53a5 and 53a6, J. Comput. Chem. 25 (13) (2004) 1656–1676.
[29] G. Bussi, D. Donadio, M. Parrinello, Canonical sampling through velocity rescaling, J. Chem. Phys. 126 (2007) 014101.
[30] B. Hess, H. Bekker, H. Berendsen, J. Fraaije, Lincs: a linear constraint solver for molecular simulations, J. Comput. Chem. 18 (12) (1997) 1463–1472.
[31] G. Kaminski, R. Friesner, J. Tirado-Rives, W. Jorgensen, Evaluation and reparametrization of the opls-aa force field for proteins via comparison with accurate quantum chemical calculations on peptides, J. Phys. Chem. B 105 (28) (2001) 6474–6487.
[32] W. Kabsch, C. Sander, Dictionary of protein secondary structure: pattern recognition of hydrogen-bonded and geometrical features, Biopolymers 22 (12) (1983) 2577–2637.
[33] Y. Watanabe, W. Hiraoka, Y. Shimoyama, M. Horiuchi, M. Kuwabara, O. Inanami, Instability of familial spongiform encephalopathy-related prion mutants, Biochem. Biophys. Res. Comm. 366 (1) (2008) 244–249.
[34] Y. Chebaro, P. Derreumaux, The conversion of helix h2 to β-sheet is accelerated in the monomer and dimer of the prion protein upon t183a mutation, J. Phys. Chem. B 113 (19) (2009) 6942–6948.
[35] A. Barducci, G. Bussi, M. Parrinello, Well-tempered metadynamics: a smoothly converging and tunable free-energy method, Phys. Rev. Lett. 100 (2) (2008) 20603.
[36] M. Bonomi, D. Branduardi, G. Bussi, C. Camilloni, D. Provasi, P. Raiteri, D. Donadio, F. Marinelli, F. Pietrucci, R. Broglia, et al., Plumed: a portable plugin for free-energy calculations with molecular dynamics, Comput. Phys. Commun. 180 (10) (2009) 1961–1972.